The Shaped Solenoid for Muon Spectroscopy

C.W. Fabjan
CERN, Geneva, Switzerland

1. Motivation

Most of the LHC physics topics require the identification and momentum measurement of leptons. For the identification of electrons, two approaches –transition radiation and fine-grained pre–shower detection– are being actively developed [1,2]. Conceptually, these approaches should work at luminosities in excess of $L = 10^{34}$ cm^{-2} s^{-1}, but the quality of electron identification near or in the high particle–density core of energetic jets remains to be established. The momentum measurement of electrons may, however, benefit from excellent precision when using the calorimetric approach. Both, homogeneous electromagnetic detectors [3,4] (LXe or BaF_2) or sampling devices [5] will reach $\sigma/E < 1\%$ for electron energies in the 100 GeV range. Muons, on the other hand, when identified as penetrating charged particles behind a calorimeter, are practically inert to the associated particle flux and event topology. For a 'discovery machine', such as the LHC, this could be a life–saving advantage, not to be given up lightly. This ease of identification is unfortunately counterbalanced to some extent by the difficulty of achieving 'good' momentum resolution. In the LHC range of interesting muon momenta –10 GeV to approximately 2 TeV– only magnetic spectroscopy is available, setting the scale for the achievable resolution, which in practical instruments will be considerably worse than then energy resolution for electrons.

Two approaches have been extensively evaluated: iron toroids magnetized at ~ 2 T, provide a robust method using rather conventional tracking methods [6]. The achievable momentum resolution is multiple scattering, limited for $p \leq 500$ GeV/c and is given by $\sigma/p \approx 0.4/B[T] \cdot \sqrt{L[Fe(m)]}$. Alternatively, tracking in air fields, as pioneered by the L3 Collaboration [7], offers the attractive advantage of high–precision momentum analysis over a wide range of muon momenta. Both techniques are at the opposite ends of the performance spectrum: not surprisingly, the challenge of good muon spectroscopy has been met in different ways [8,9].

There has been considerable debate about the 'required' momentum resolution for muons. Typically, the Higgs $\rightarrow$ ZZ at an intermediate mass (~ 300 to 500 GeV/c^2) has been analysed. Indeed, if Nature would obligingly proceed along the lines of present-day event generators, such decays should be visible above the QCD-background, even if the resolution is $\Delta p/p \approx 0.12$. What happens, however, if the branching ratios into ZZ are smaller than assumed [10]? Better resolution would help. There are other cases which argue for better resolution: in the Standard Model the Higgs mass is evaluated to be below $M < 200$ GeV/c^2, and its detection will tax the resolution of any detector. At the high-mass end of the LHC discovery potential, other mechanisms responsible for the breaking of the electroweak symmetry may manifest themselves, e.g. as a WZ final state. Study of this reaction again requires good momentum resolution. There may be several generations of Zs: the mass reach of the LHC is approximately 4 TeV/c^2, limited by the signal-to-background ratio, i.e. the momentum resolution. The list is not complete.

In this note, we comment on the two principal ingredients of air-field spectroscopy: the magnet and the tracking possibilities. Whilst the concept is that of the L3 and L* Collaborations [11], the detailed approach is different and may offer experimental advantages.

High-precision muon spectroscopy is arguably the single most important detection technique to be developed for the LHC: competing concepts should be evaluated to understand their technical and financial dimensions. In my view this is the pre-requisite for an informed decision on the muon systems for our LHC detectors.

2. The Shaped Solenoidal Magnet

One major difficulty, characteristic of LHC experimentation, is the requirement of large rapidity coverage. For electrons and muons, a coverage of $|\eta| < 2.5$ is considered adequate, although by no means generous. The magnetic coverage does not come easily: in the L*-approach, the central solenoid, providing good momentum resolution for $|\eta| < 1.5$, is complemented by additional muon spectrometers covering the larger rapidity regions.

The concept discussed here has a long history: it dates back to the development of the 'Open Axial Field Magnet' conceived by T. Taylor for the Axial Field Spectrometer at the ISR [12], as shown in Fig. 1. This concept was further extrapolated to several interesting magnet configurations, as discussed in Ref. [13]. More recently, the 'shaped solenoid' was adapted to the supercollider requirements [14], as indicated in Fig. 2. A warm solenoidal coil is implied. Field shaping is accomplished, both by increasing the current density at the ends and by extending the yoke into cones for improved flux bending at small polar angles. Considerable bending power is possible with this arrangement, down to $|\eta| \leq 2.5$, see Fig. 3.

A variation of this concept is shown in Fig. 4. Six discrete superconducting coils are distributed to provide field shaping over $|\eta| \leq 2.3$, as can be inferred from the bending power, Fig. 5. Assumed current densities (5 A/mm^2 in the large coils, 20 A/mm^2 in the two small coils) allow for established conductor technology. The overall diameter of the magnet, including the return yoke, is approximately 20 m: it would still fit into a 'standard' longitudinal interaction region for which a maximum diameter of 24 m is considered acceptable [15]. The cylindrical yoke contains approximately 25,000 t of iron; the two forward portions each weigh approximately 4500 t. Hence the total weight is similar to that of a shallow (3 m deep) iron toroid for an inner detector of comparable size [6]. A potential simplification may be achieved in the construction of the central iron yoke: it could be assembled from extruded iron bars, requiring no further machining, and could be part of the structural support of the cylindrical walls of the experimental hall.

3. The Tracking Detector

The requirements on the tracking system can be gauged from Fig. 5. At $\theta = 90^o$, a 1 TeV muon would have a sagitta of ~ 0.6 mm. A 50 μm error on the sagitta measurement would provide 8% resolution at 1 TeV.

The L3 Collaboration has demonstrated that an effective spatial resolution of $\sigma \approx 50$ μm may be achieved with multiple measurements using drift–chamber techniques, where each individual measurement has typically an error of $\sigma \approx 200$ μm [7]. The drift–chamber concept may, however, be quite difficult to implement in the present magnet design, owing to the field shaping as a function of polar angle.

We are attracted by three recent developments in gaseous trackers: microstrip avalanche chambers [16], pad chambers [17] and straw chambers. In the first two techniques, the position is measured by the hit pattern of anode strips [16] or cathode segments [17,18]. Conceptually, control of systematic effects is provided by depositing the sensor elements on inherently stable substrates, e.g. quartz plates.

The microstrip avalanche chambers have not yet been fabricated in large (~ 1 m^2) size, but fabrication techniques (photolithography) used for the present, successfully operated detectors, would allow devices to be constructed in dimensions of up to 40 x 40 cm^2. Assuming anode strip lengths of ~ 50 cm with 200 μm centre spacing (providing a spatial resolution of ≈ 60 μm), the total channel count would reach $N \approx 3 \times 10^7$. The required electronics is very similar to the electronics used at present for Si–strip detectors (with the addition of input spark protection). Strips would be ganged to form 'FAST ORs' available for trigger information. Given the very low occupancy, extensive multiplexing would be used to transfer the hit pattern to the DAQ system.

The second approach uses the interpolation of cathode strips, oriented perpendicularly to the direction of the anode wires. Interpolation accuracies of 1% of the readout spacing have been reported [17,18]. For the muon chambers, we would like to use rather long (~ 50 cm) strips, resulting in a noise penalty and possibly in a reduced interpolation accuracy. Assuming 3 mm wide interpolation, a total of $N \approx 2 \times 10^6$ channels would be required. Fast ORs would provide trigger capability and extensive multiplexing would permit a 'reasonable' ($\approx 10^4$?) channel count of digitization electronics. These chambers would be tilted by the Lorentz angle with respect to normal incidence to achieve approximately perpendicular charge collection, minimizing the effect of Landau fluctuations on the position resolution. It will be advantageous to use Xe/CO_2 mixtures, both to increase the collected charge and to benefit from the relatively small Lorentz angle [19] ($\theta_L \approx 16°$ at 1 T).

The third approach returns to the time–honoured concept of drift chambers, using their modern incarnation of 'drift–straws' [20]. These detector elements have typical diameters of 5 to 10 mm and are frequently thin–walled made from material, such as Mylar or Kevlar. Stable operation is achieved with a variety of gas–mixtures [Ar/Ethane, Ar/C02/CH4, Di–Methyl–ether] (DME). Spatial resolutions of $\sigma \approx 50$ μm at 1 atm, improving to $\sigma < 30$ μm for operation at 4 atm. have been measured. Considerable operational experience has been obtained with vertex chambers operated at several e^+e^- colliders. Several groups have evaluated the use of such detector elements for a large central tracker for SSC experiments. We imagine th euse of thin–walled aluminum tubes, 8 to 10 mm in diameter, operated at a few bars with DME, potentially providing a spatial resolution of $\sigma \approx 30$ μm for a single measurement. Coarse second–coordinate readout may be obtained by measuring the arrival time at both ends of a tube.

Needless to say, the first two concepts would require extensive work before they could be considered as tracking candidates. The third concept is a much more mature technique. Developments would concentrate on fabrication techniques, drift stability and systems aspects.

4. The Muon–Chamber Space Frame

A conceptual detector layout is shown in Fig. 6. The cylindrical yoke is seen to support the central (~ 3000 t) detector on support rods, possibly arranged as spokes of a bicycle wheel. It is a matter of detailed engineering analysis to understand whether the support of the central detector is independent (as in L*) or integrated with the muon–chamber support, as indicated in Fig. 6.

Whether both functions are integrated or not, the muon–chamber space frame is constructed from materials with coefficients of thermal expansion (CTE) = 0 in the temperature range of operation. In recent years, a number of novel composite materials have become available, combining high strength, stiffness, and relatively low atomic number (long radiation length) with zero CTE [19]. In this approach, one would aim for an overall long term (24 h) stability of the space frame of $\sigma \approx 100$ µm, consistent with the measured position stability of the LEP machine components [20]. If this level could be achieved, it would seem adequate to monitor the position of the muon chambers passively and to use the deviations from nominal position as correction terms in the reconstruction programme.

5. Conclusions

High precision muon spectroscopy should be part of an LHC experiment. A magnet concept combined with recently developed gaseous tracking detectors is discussed, which would satisfy the resolution requirements. In a next step, the engineering aspects of the magnet would have to be evaluated. Concurrently, a R&D programme would be needed to study the tracking performance of a module in a magnetic field, using the support techniques briefly outlined.

I would like to thank the many colleagues who discussed these concepts with me and in particular, T. Tortschanoff who carried out the magnetic field calculations for the superconducting version.

References

[1] V.A. Polychronakos et al., Integrated High–Rate Transition Radiation Detector and Tracking Chamber for the LHC; Proposal CERN/DRDC/90–38 (1990).

[2] D.J. Munday et al.: A Proposal to Study a Tracking/Preshower Detector for the LHC; CERN/DRDC/90–27 (1990).

[3] M. Chen et al., Nucl. Instrum. and Methods A267 (1988) 43.

[4] H. Newman et al.: R&D Proposal for Fast and Radiation Hard Crystal Calorimeter at LHC; CERN/DRDC/90–54.

[5] C.W. Fabjan, Sampling Calorimeters vs Homogeneous Total Absorption Calorimeters: a Performance Comparison. Invited talk, Conference on Very High Resolution Electromagnetic Calorimetry, November 1989, Sigtuna, Sweden.

[6] G. Carboni, these proceedings.

[7] B. Adeva et al., Nuclear Instrum. Methods A289 (1990) 35.

[8] M. Della Negra et al., Study of Muon Triggers and Momentum Reconstruction in a Strong Magnetic field, CERN/DRDC/90–26 (1990).

[9] U. Goerlach, these proceedings.

[10] These proceedings.

[11] L. Baksay et al., Expression of Interest by the L* Collaboration.

[12] H. Gordon et al., Nuclear Instrum. Methods 196 (1982) 303.

[13] T. Taylor, Physica Scripta, 23 (1981) 459.

[14] E. Dolgosheina, T. Taylor and W.J. Willis, Field Shaping by Iron for Muon Measurement at Hadron Colliders, to be published in Nuclear Instrum. and Methods, 1990.

[15] L. Leistam, the proceedings.

[16] A. Oed, Nucl. Instrum. Methods A263 (1988) 351;
F. Angelini et al., Particle World 1 (1990) 85.

[17] R. Debbe et al., BNL 43405 (1990).

[18] H. Beker et al., Nucl. Instrum. Methods A283 (1989) 762.

[19] H. Daum et al., Nucl. Instrum. Methods 152 (1978) 541.

[20] W.H. Toki, Review of Straw Chambers, SLAC–PUB–5232 and Proc. 5th Int. Conf. on Instrumentation for Colliding Beam Physics, Novosibirsk, 1990 (to be published).

Figure Captions:

Fig. 1 Vertical cross–section through the open axial field magnet. The magnetic field lines show the direction and level of the field useful for momentum analysis and also the level of 'stray field' in the external detectors [12].

Fig. 2 Cross–section through magnet with shaped iron poles; the field lines are also shown indicating the effect on the magnetic field by the forward cones of the magnet yoke [14].

Fig. 3 Display of BL^2 (Tm^2) for the magnet displayed in Fig. 2 [14].

Fig. 4 Schematic layout of the shaped iron yoke and six superconducting coils.

Fig. 5 Integral $\overline{BL^2}$ of the magnet shown in Fig. 4 (left ordinate and solid line) and the sagitta for 1 TeV particles (right ordinate and dashed line).

Fig. 6 Conceptual layout of a muon spectrometer inside the superconducting shaped solenoid.

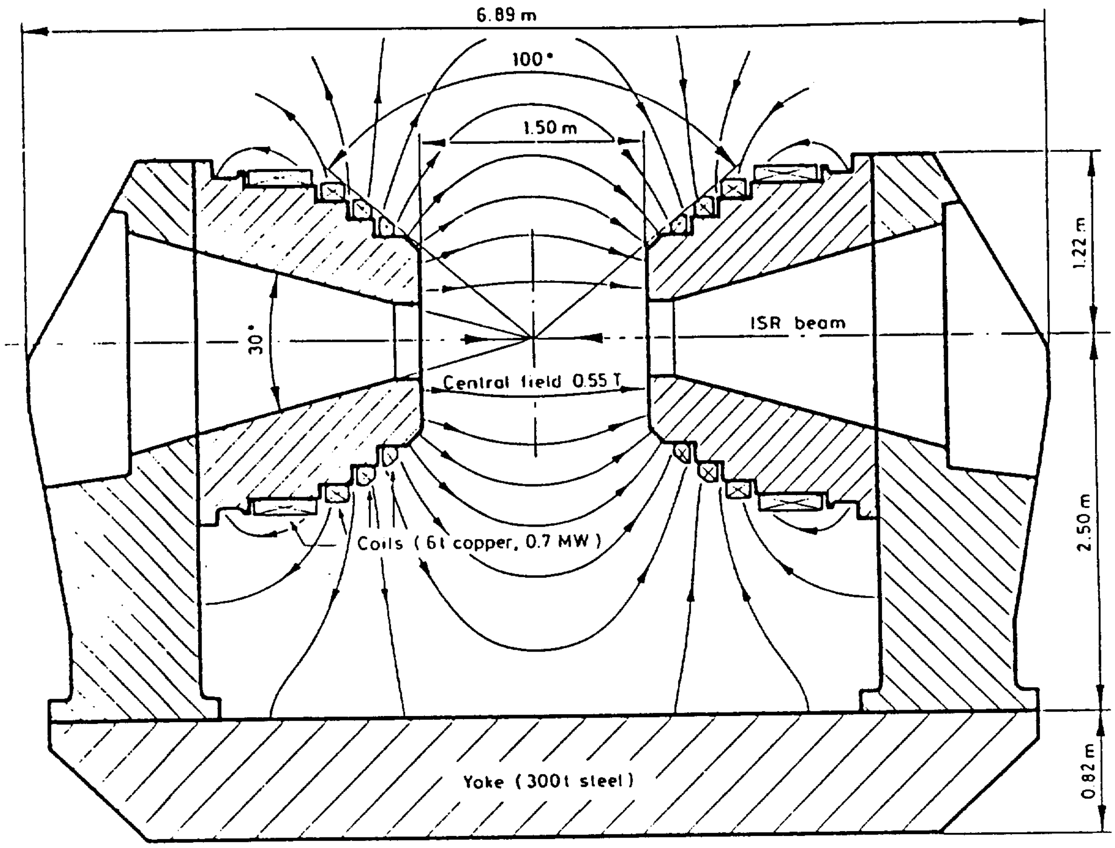
6.89 m
100°
1.50 m
30°
ISR beam
Central field 0.55 T
Coils (6 t copper, 0.7 MW)
Yoke (300 t steel)
1.22 m
2.50 m
0.82 m

Fig. 1

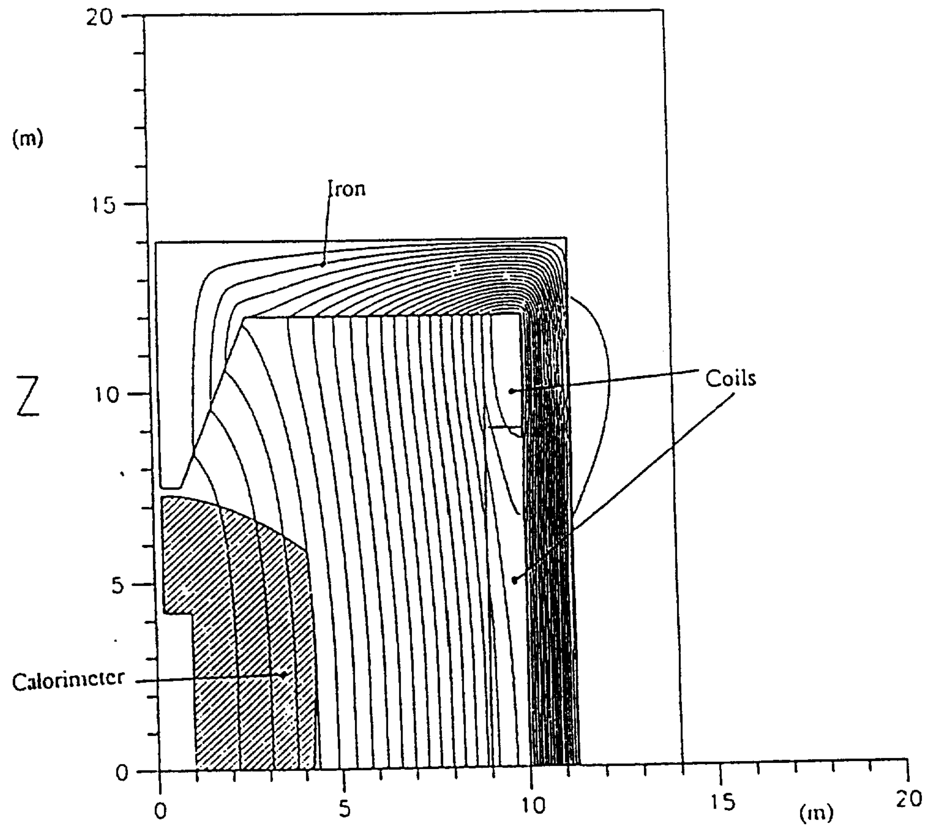
Z
(m)
Iron
Coils
Calorimeter
R
(m)
0
5
10
15
20

Fig. 2

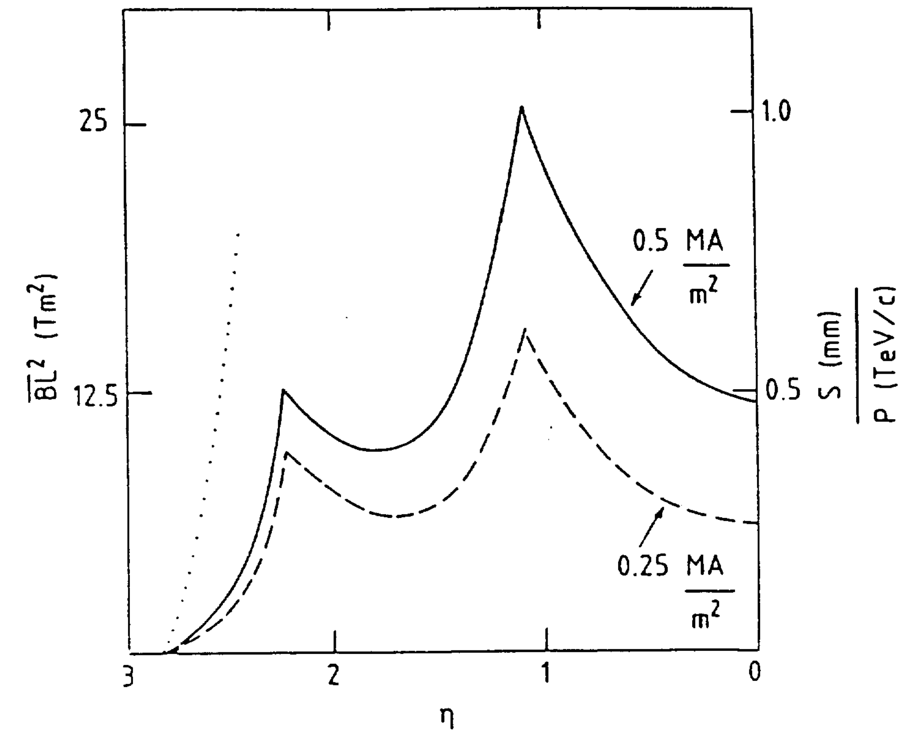
25
12.5
$\overline{BL}^2$ (Tm^2)
1.0
0.5
$\frac{S \text{ (mm)}}{P \text{ (TeV/c)}}$
0.5 $\frac{MA}{m^2}$
0.25 $\frac{MA}{m^2}$
3
2
1
0
η

Fig. 3

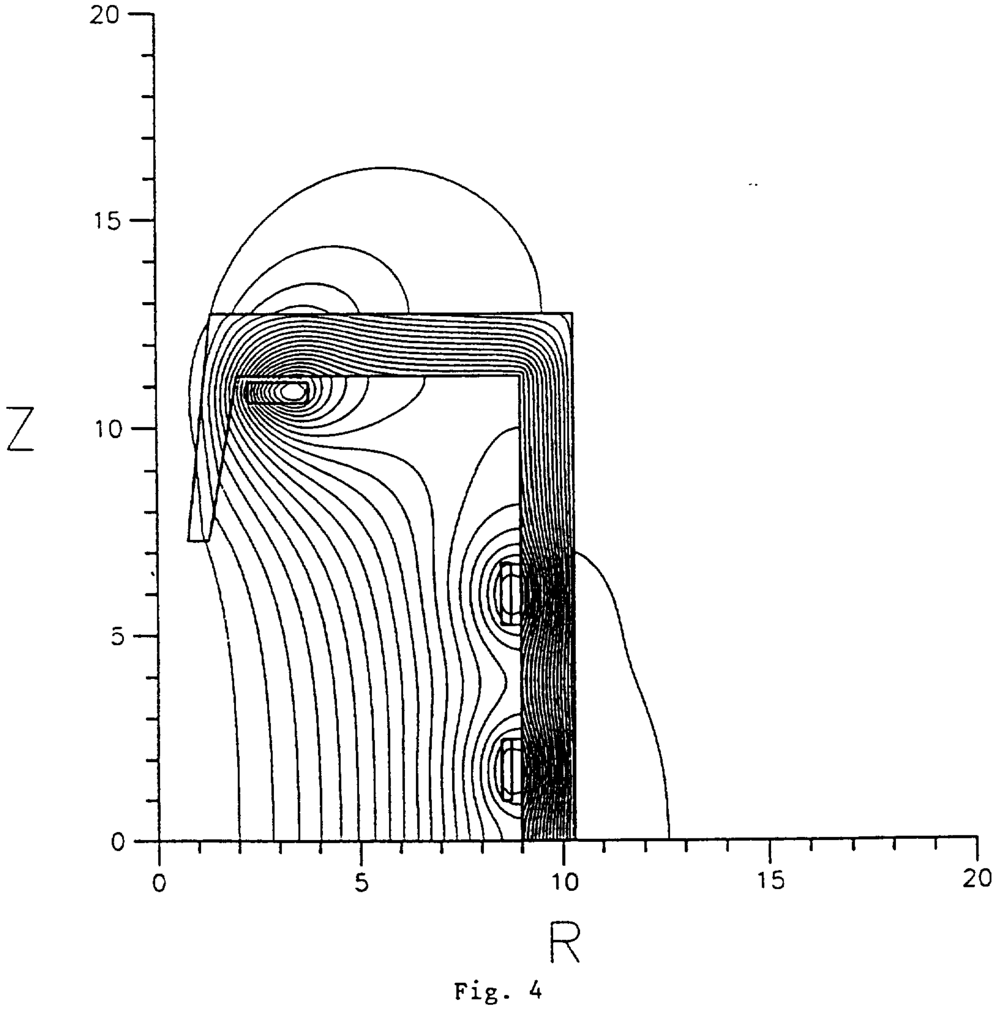
20
15
10
5
0
Z
0
5
10
15
20
R

Fig. 4

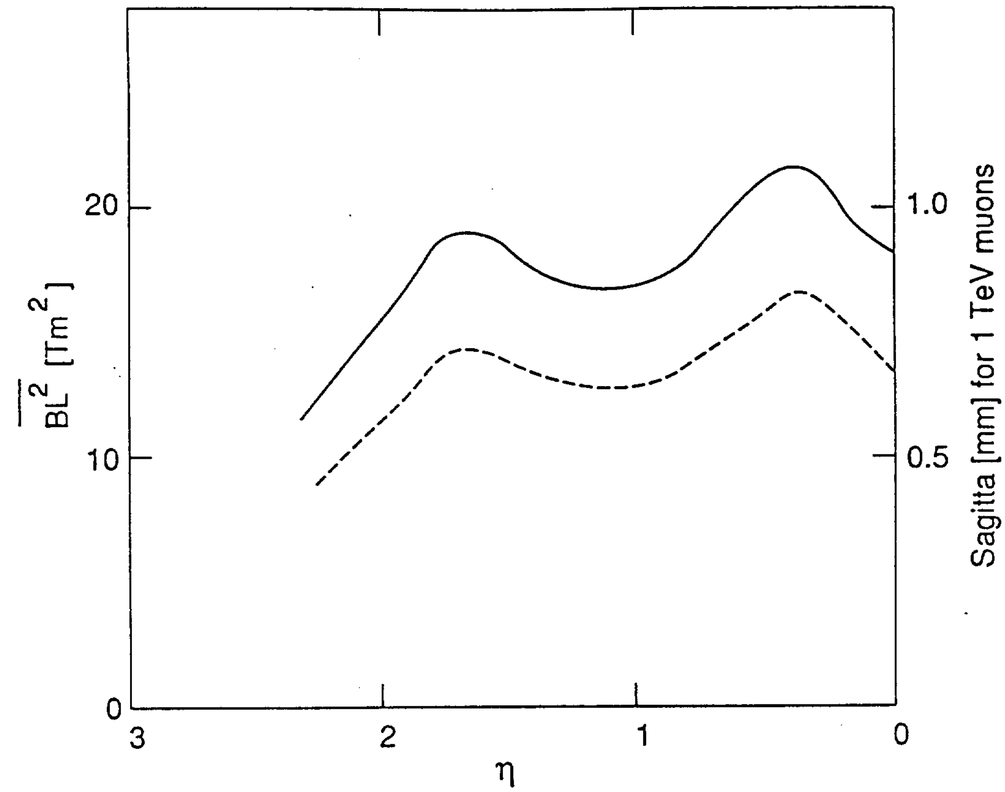

20
10
0
3
2
1
0
η
$\overline{BL^2}$ [Tm^2]
1.0
0.5
Sagitta [mm] for 1 TeV muons

Fig. 5

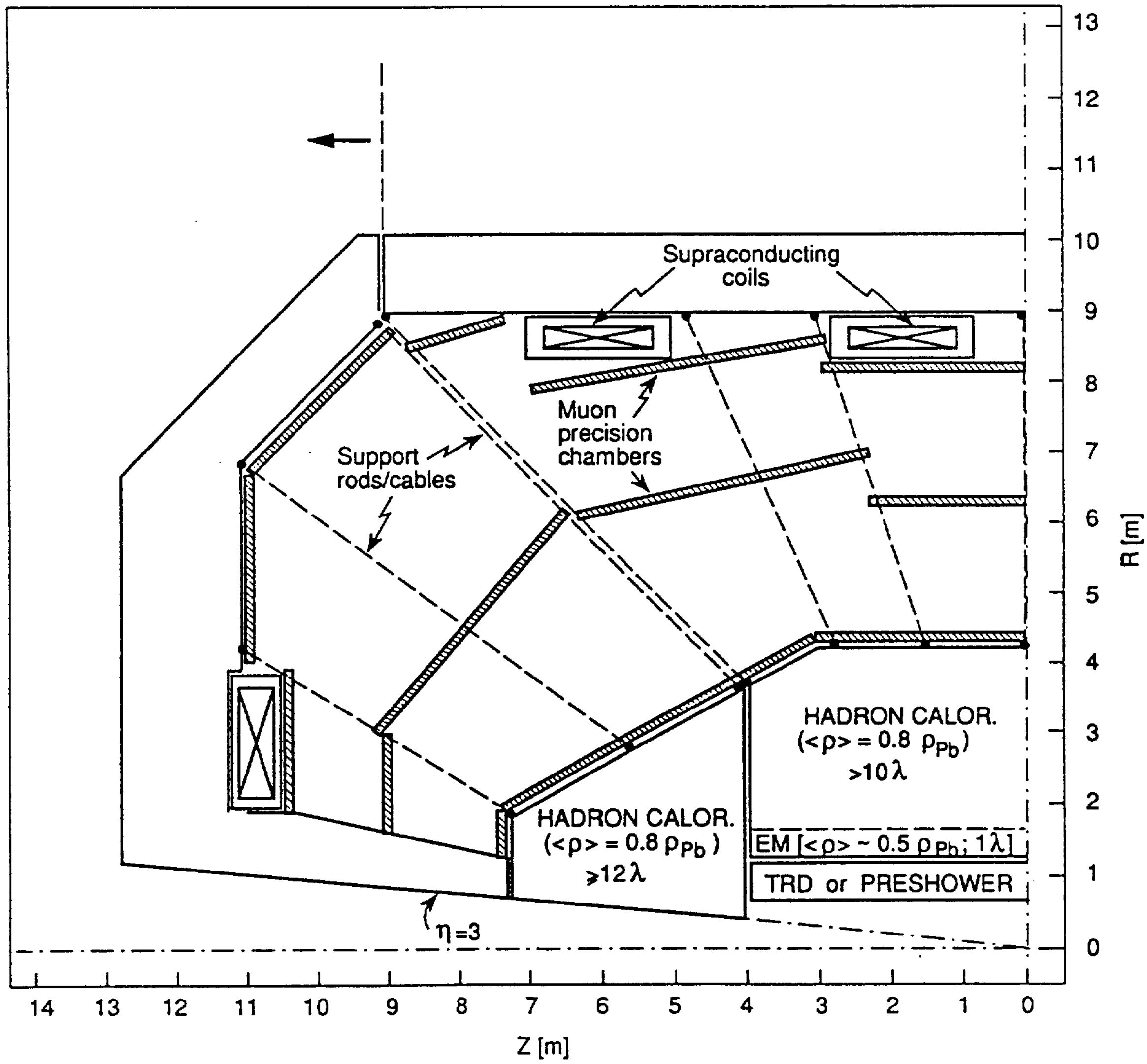

Supraconducting coils
Muon precision chambers
Support rods/cables
HADRON CALOR. (<ρ> = 0.8 ρ_{Pb}) >10λ
HADRON CALOR. (<ρ> = 0.8 ρ_{Pb}) ≥12λ
EM [<ρ> ~ 0.5 ρ_{Pb}; 1λ]
TRD or PRESHOWER
η=3
R [m]
Z [m]

Fig. 6